Electronic Supplementary Material (ESI) for Journal of Materials Chemistry A.
This journal is © The Royal Society of Chemistry 2016

Supporting Information

Artificially-engineered, bicontinuous anion-conducting/-repelling polymeric phases as a selective ion transport channel for rechargeable zinc-air battery separator membranes

Hyun-Woo Kim[a], Jun-Muk Lim[a], Hyeon-Ji Lee[a], Seung-Wook Eom[b], Young Taik Hong[c] and Sang-Young Lee*[a]

[a]*Department of Energy Engineering, School of Energy and Chemical Engineering, Ulsan National Institute of Science and Technology (UNIST), Ulsan, 689-798, Korea*
[b]*Battery Research Center, Korea Electrotechnology Research Institute (KERI), Changwon, 641-120, Korea*
[c]*Energy Materials Research Center, Korea Research Institute of Chemical Technology (KRICT), Daejeon, 305-600, Korea*

Figure S1. Assembly diagram of a Zn-air cell suggested in this work, wherein the major cell components were integrated in the following order: Zn anode electrodeposited on a nickel plate, separator membrane, and air cathode.

Figure S2. SEM images (upper row) and chemical stability in 6M KOH electrolyte solution (lower row) of PVA/PAA nanofiber mat as a function of PVA/PAA composition ratio: (a) PVA/PAA = 5/5 (w/w); (b) 7/3; (c) 9/1.

Figure S3. Effect of annealing environment (air vs. Ar, at 120 ^{o}C) on chemical degradation of Nafion-impregnated PVA/PAA nanomat: (a) photographs; (b) TGA profiles.

Figure S4. (a) SEM images of microporous PP separator (Celgard3501). (b) A photograph showing mechanical flexibility of Celgard3501.

Figure S5. Tensile properties of PBE membrane and Celgard3501: (a) stress-strain curve; (b) summary of major tensile characteristics of the membranes.

Figure S6. Nyquist plots used for estimating ionic conductivity of: (a) Celgard3501; (b) Nafion film; (c) PVA/PAA film; (d) PBE membrane.

Figure S7. (a) A diffusion cell used for measurement of OH^- transference number. (b) Comparison of OH^- transference number between different membranes.

Figure S8. Photographs showing the crossover of blue dye through PBE membrane and Celgard3501.

Figure S9. Voltammogram profiles (scan rate = 5 mV s^{-1}) of Celgard3501 and PBE membrane, revealing no appreciable decomposition of any components in the PBE membrane takes place within the operating voltage range (vs. Pt/Pt^{2+}).

Figure S10. Video clips showing the operation of hypnosis-spiral wheels connected to Zn-air cells incorporating: (a) Celgard3501; (b) PBE membrane.

Figure S11. Electrochemical activity of Zn-air cells incorporating the reused separator membranes. (a),(b) For the reused Celgard3501 (obtained after the cycle time of 900 min in

the 1st cell): (a) galvanostatic charge/discharge profiles of the 2nd cell; (b) SEM and EDS images of the air cathode surface after the 2nd cycling test. (c),(d) For the reused PBE membrane (obtained after the cycle time of 2500 min in the 1st cell): (c) galvanostatic charge/discharge profiles of the 2nd cell; (d) SEM and EDS images of the air cathode surface after the 2nd cycling test.

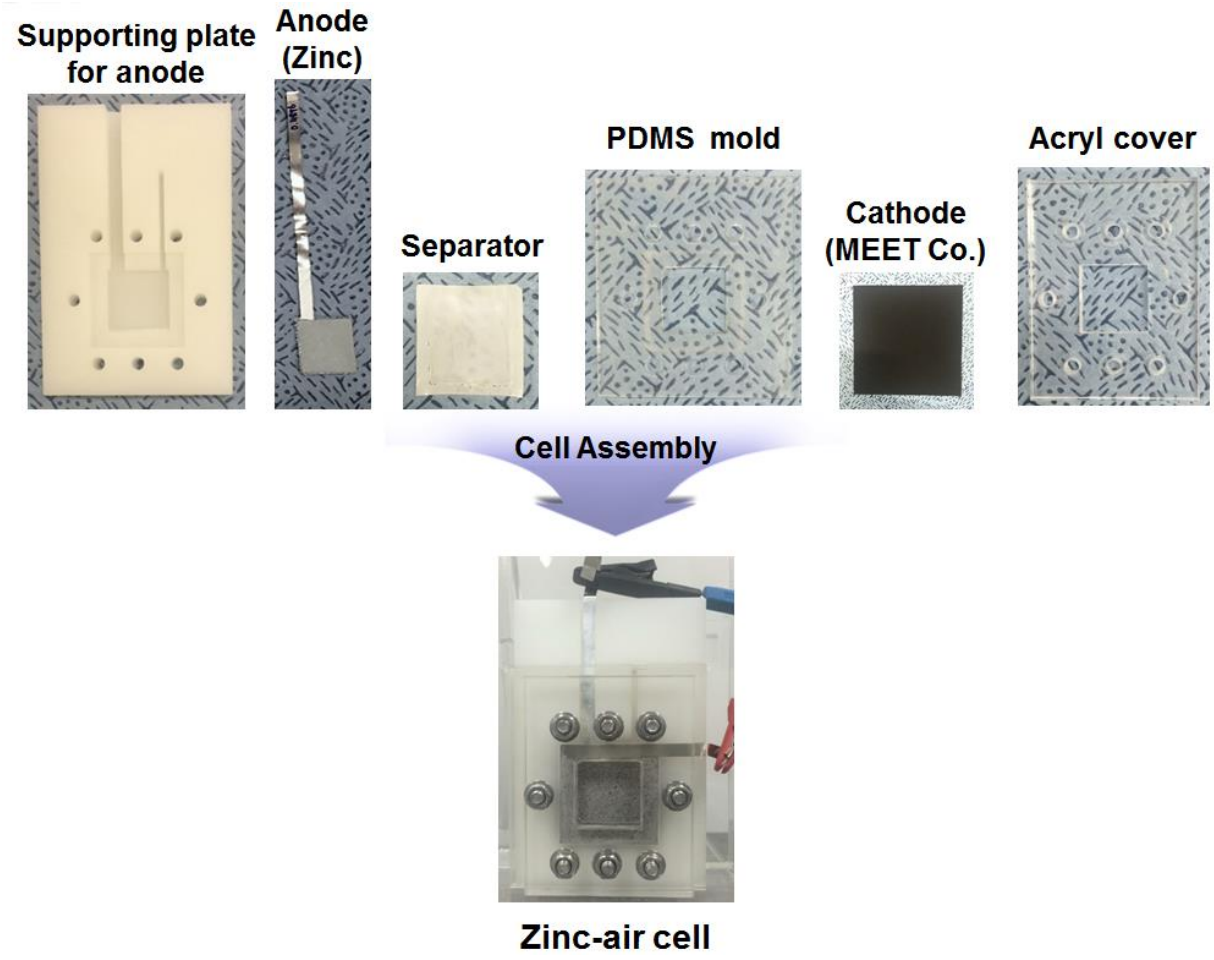

Figure S1. Assembly diagram of a Zn-air cell suggested in this work, wherein the major cell components were integrated in the following order: Zn anode electrodeposited on a nickel plate, separator membrane, and air cathode.

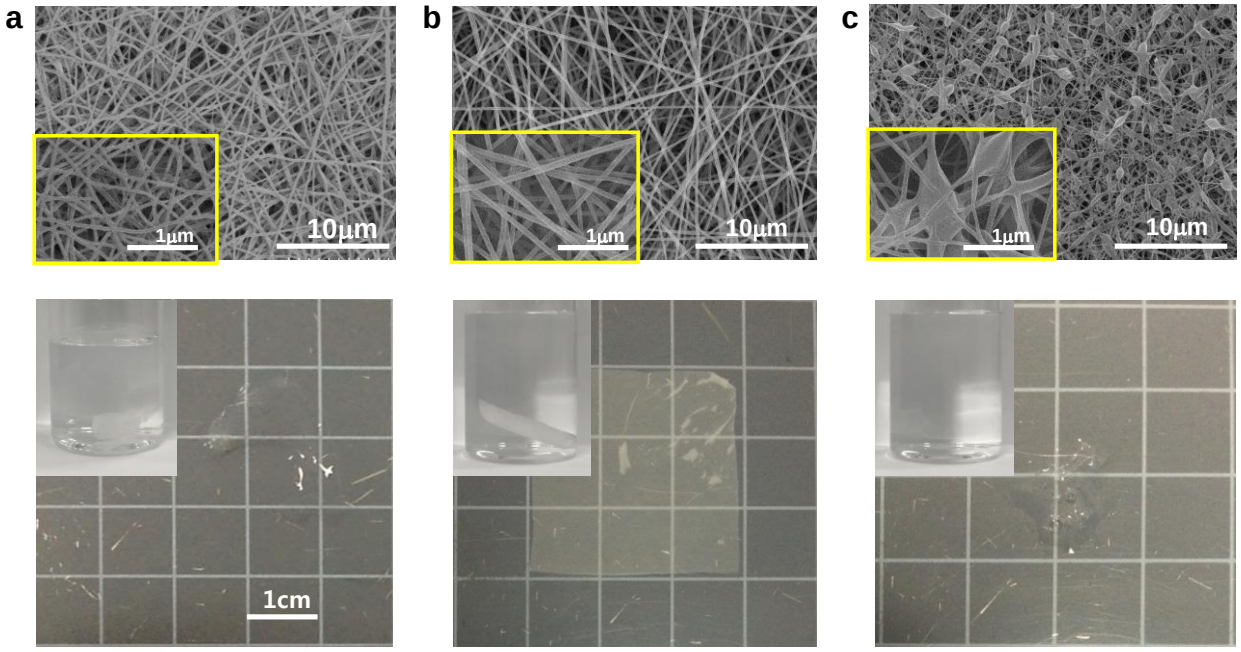

Figure S2. SEM images (upper row) and chemical stability in 6M KOH electrolyte solution (lower row) of PVA/PAA nanofiber mat as a function of PVA/PAA composition ratio: (a) PVA/PAA = 5/5 (w/w); (b) 7/3; (c) 9/1.

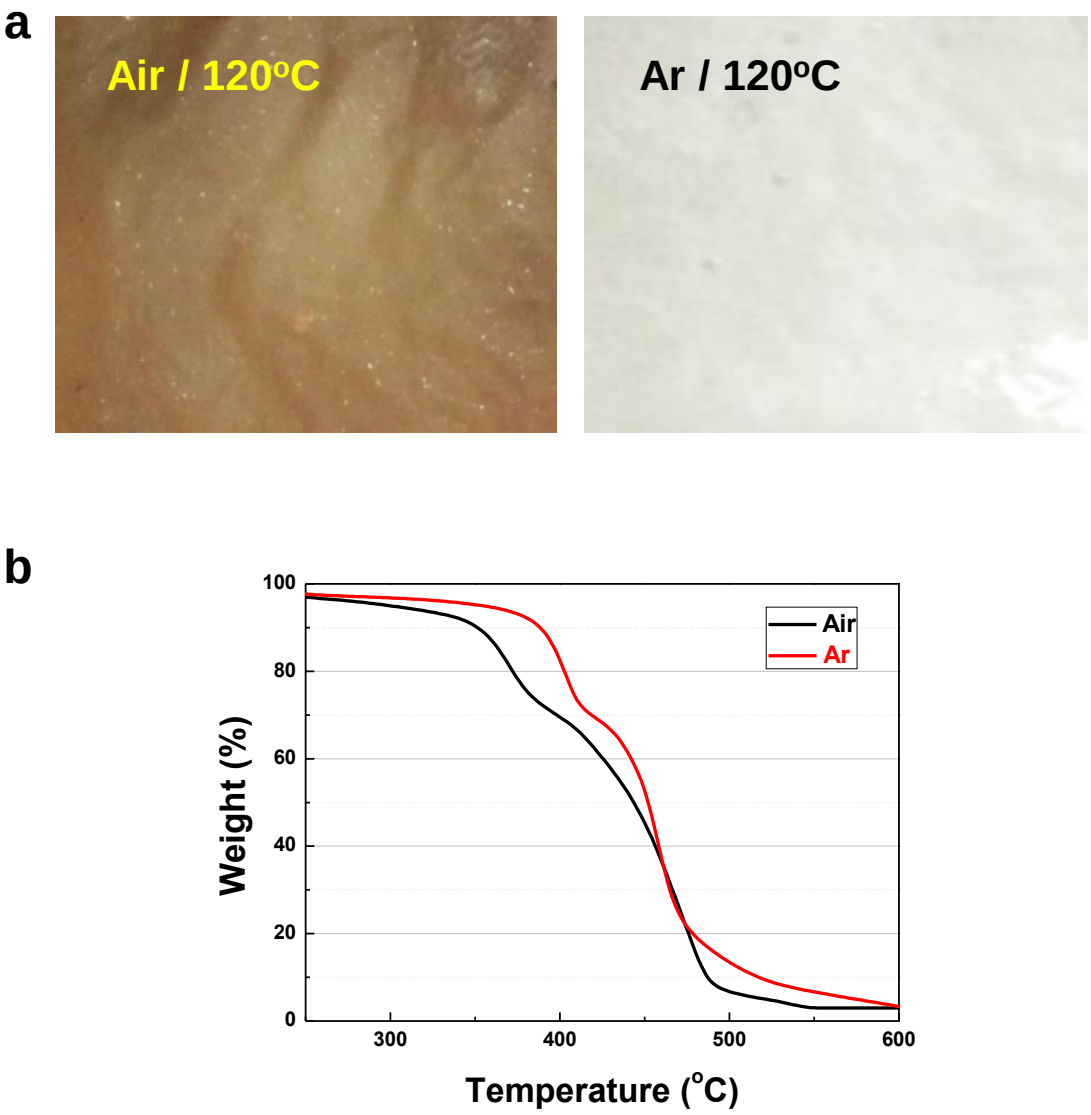

Figure S3. Effect of annealing environment (air vs. Ar, at 120 ^{o}C) on chemical degradation of Nafion-impregnated PVA/PAA nanomat: (a) photographs; (b) TGA profiles.

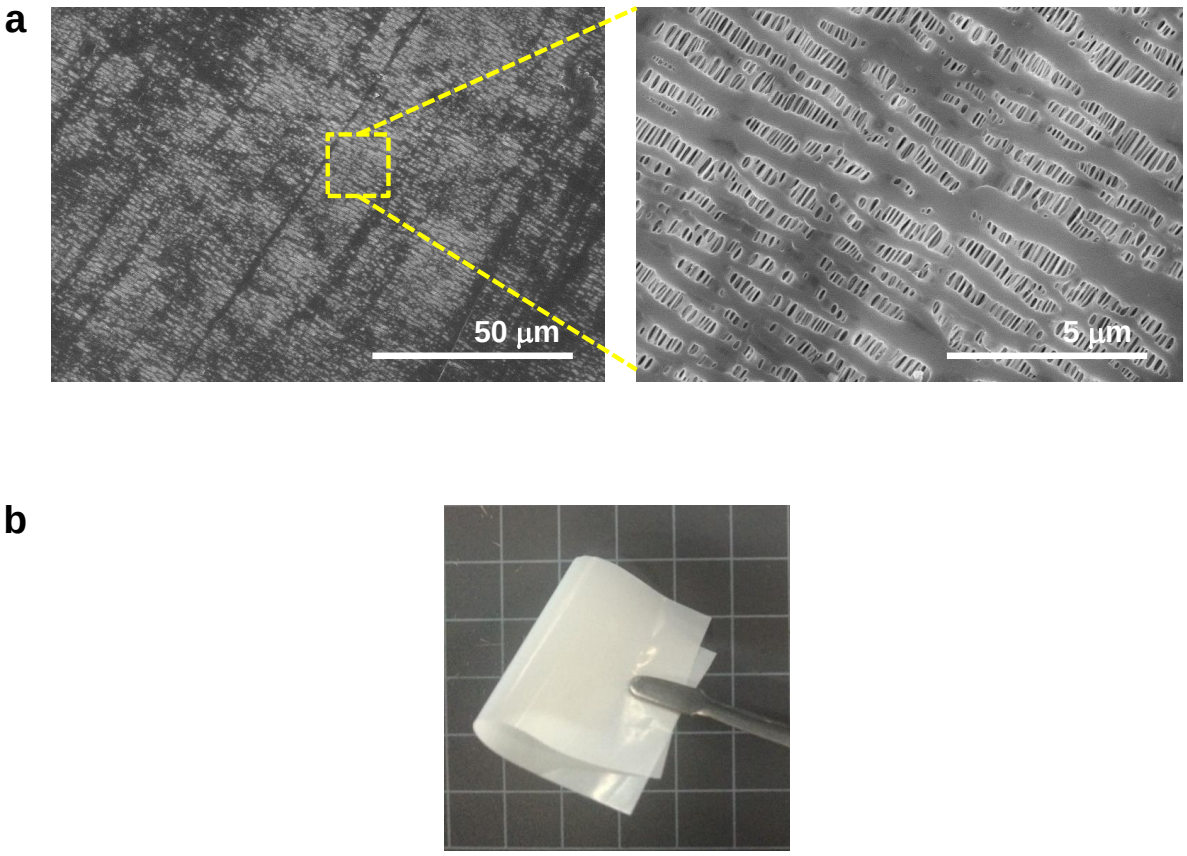

Figure S4. (a) SEM images of microporous PP separator (Celgard3501). (b) A photograph showing mechanical flexibility of Celgard3501.

a

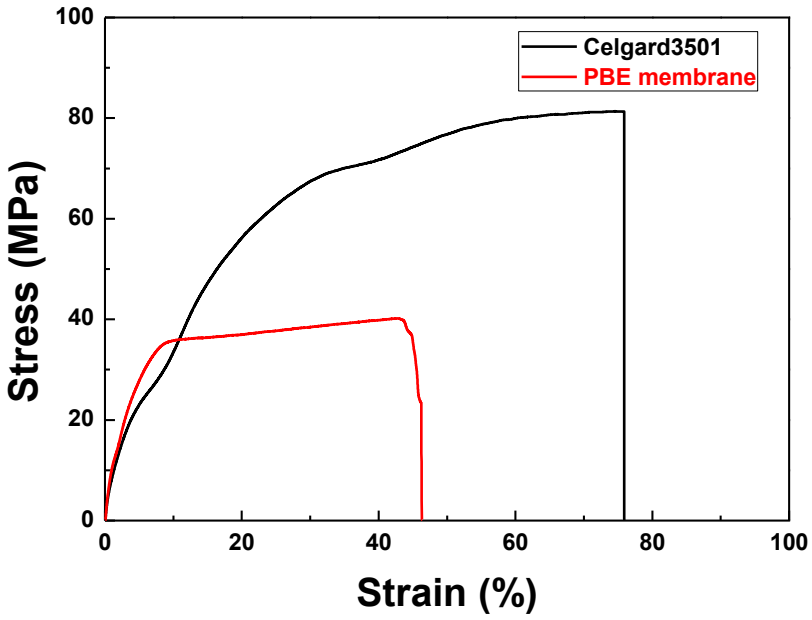

b

	Tensile Strength / MPa	Elongation at Break / %	Tensile Modulus / MPa
Celgard3501	81.3	75.9	751.4
PBE membrane	39.4	46.2	973.1

Figure S5. Tensile properties of PBE membrane and Celgard3501: (a) stress-strain curve; (b) summary of major tensile characteristics of the membranes.

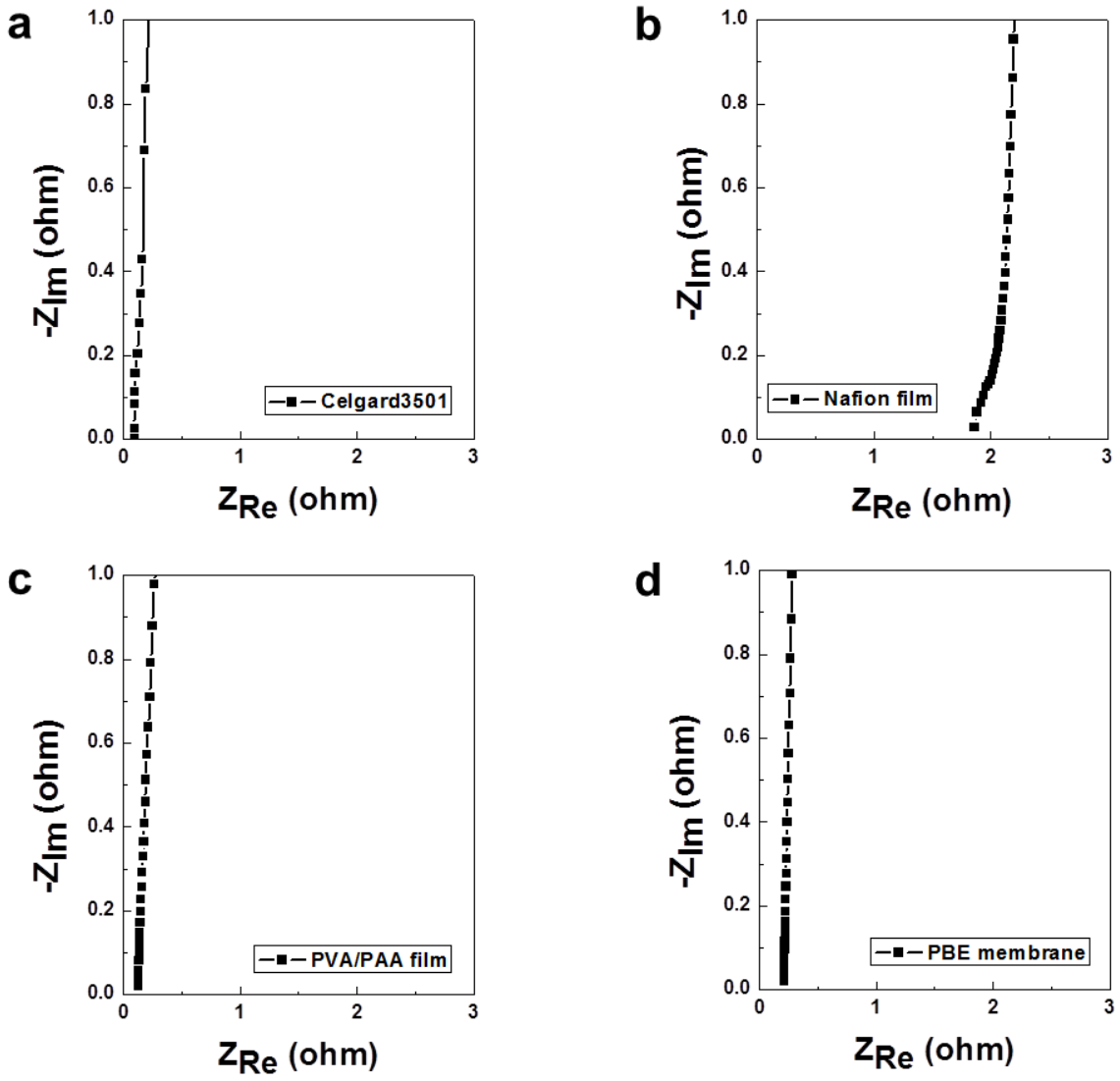

Figure S6. Nyquist plots used for estimating ionic conductivity of: (a) Celgard3501; (b) Nafion film; (c) PVA/PAA film; (d) PBE membrane.

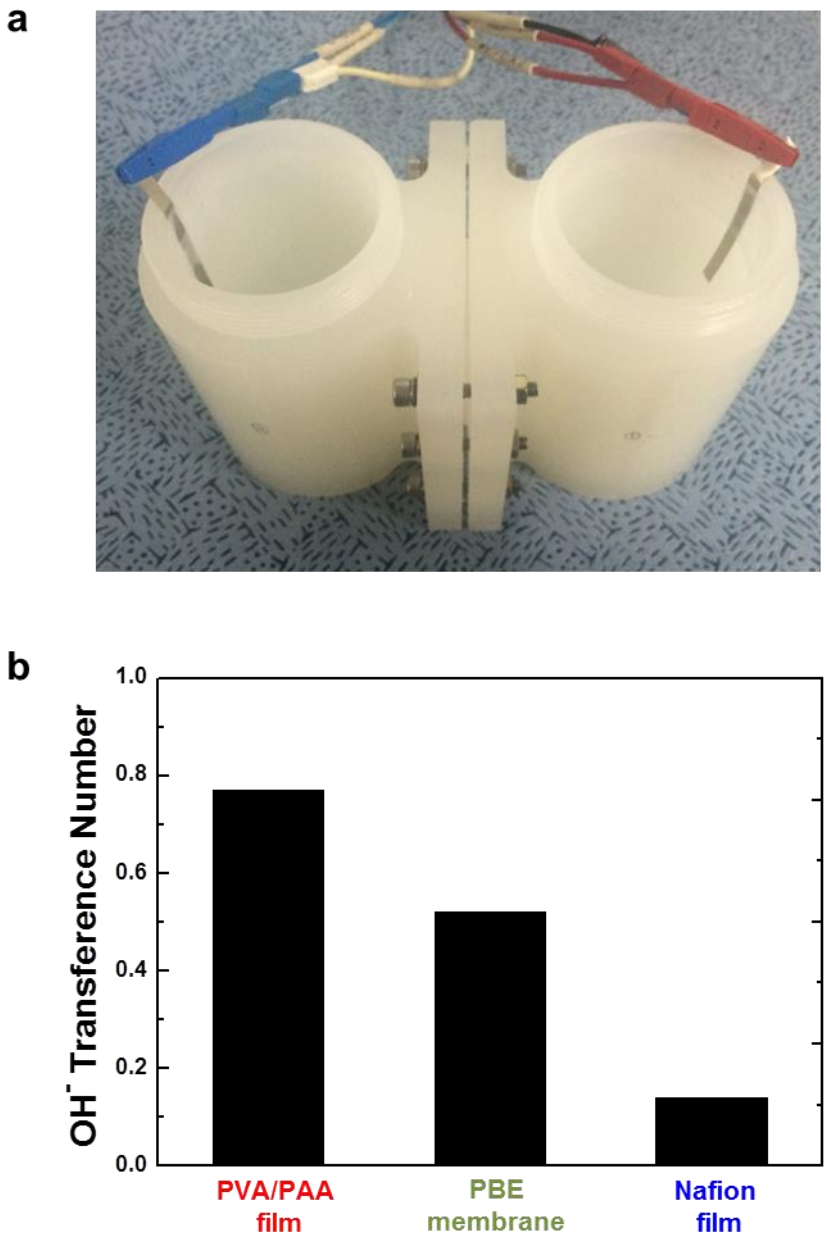

Figure S7. (a) A diffusion cell used for measurement of OH^- transference number. (b) Comparison of OH^- transference number between different membranes.

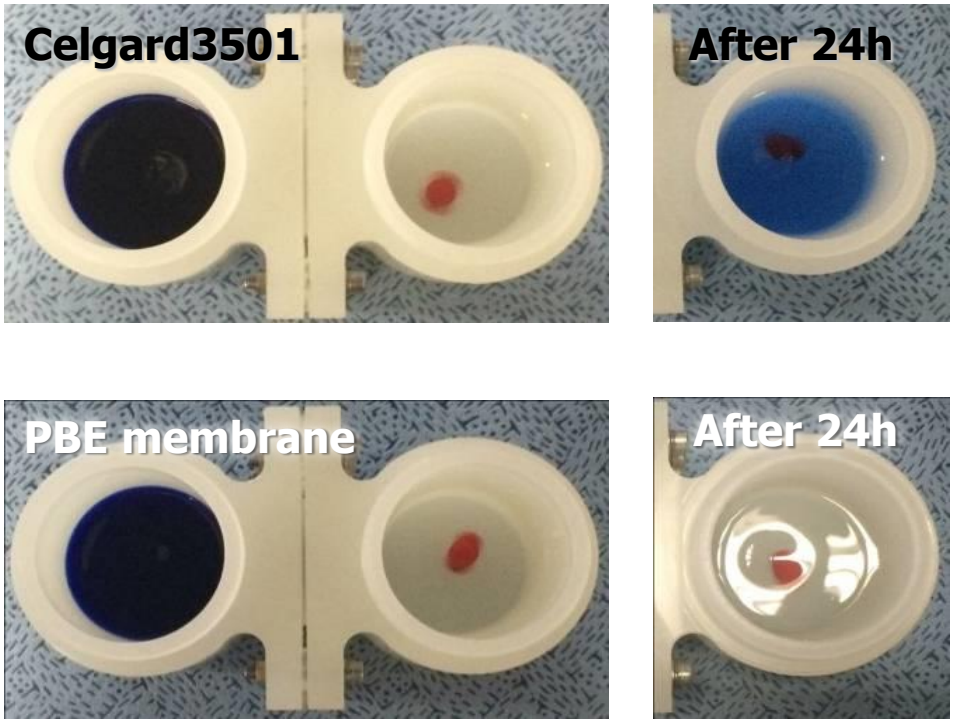

Figure S8. Photographs showing the crossover of blue dye through PBE membrane and Celgard3501.

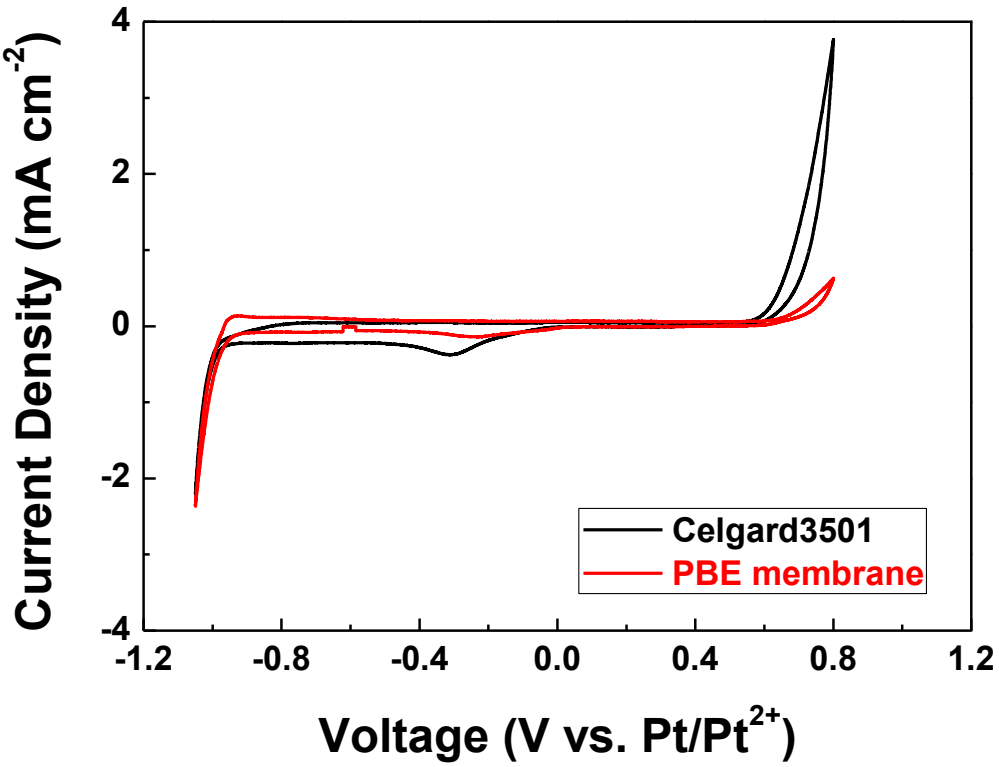

Figure S9. Voltammogram profiles (scan rate = 5 mV s^{-1}) of Celgard3501 and PBE membrane, revealing no appreciable decomposition of any components in the PBE membrane takes place within the operating voltage range (vs. Pt/Pt^{2+}).

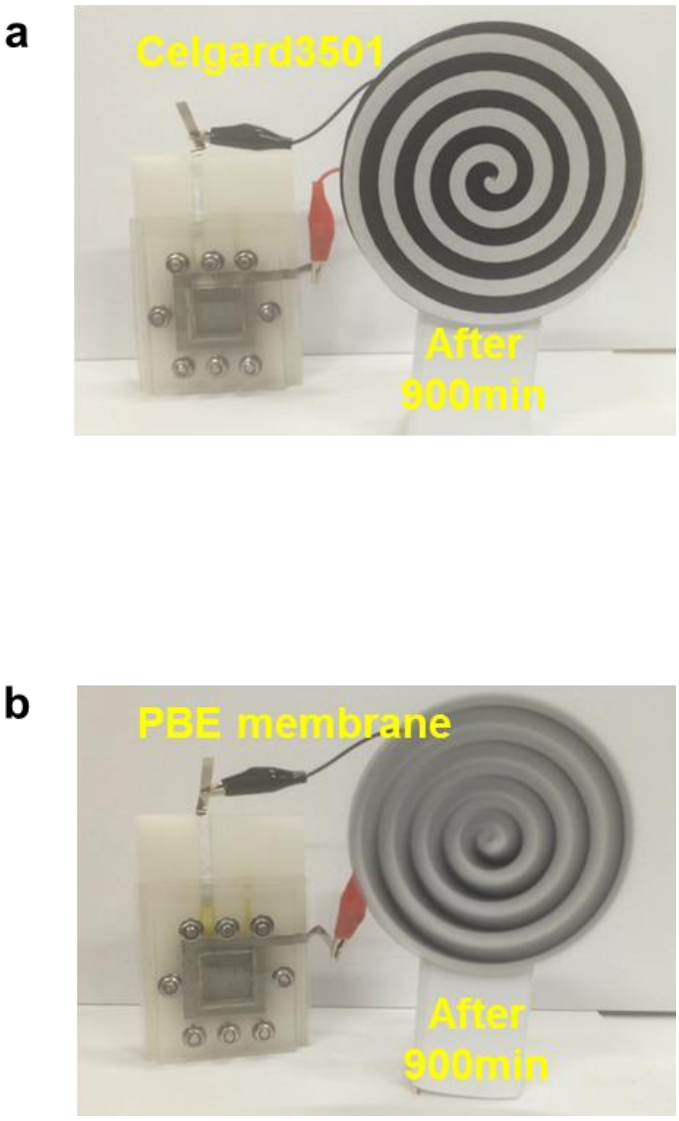

Figure S10. Video clips showing the operation of hypnosis-spiral wheels connected to Zn-air cells incorporating: (a) Celgard3501; (b) PBE membrane.

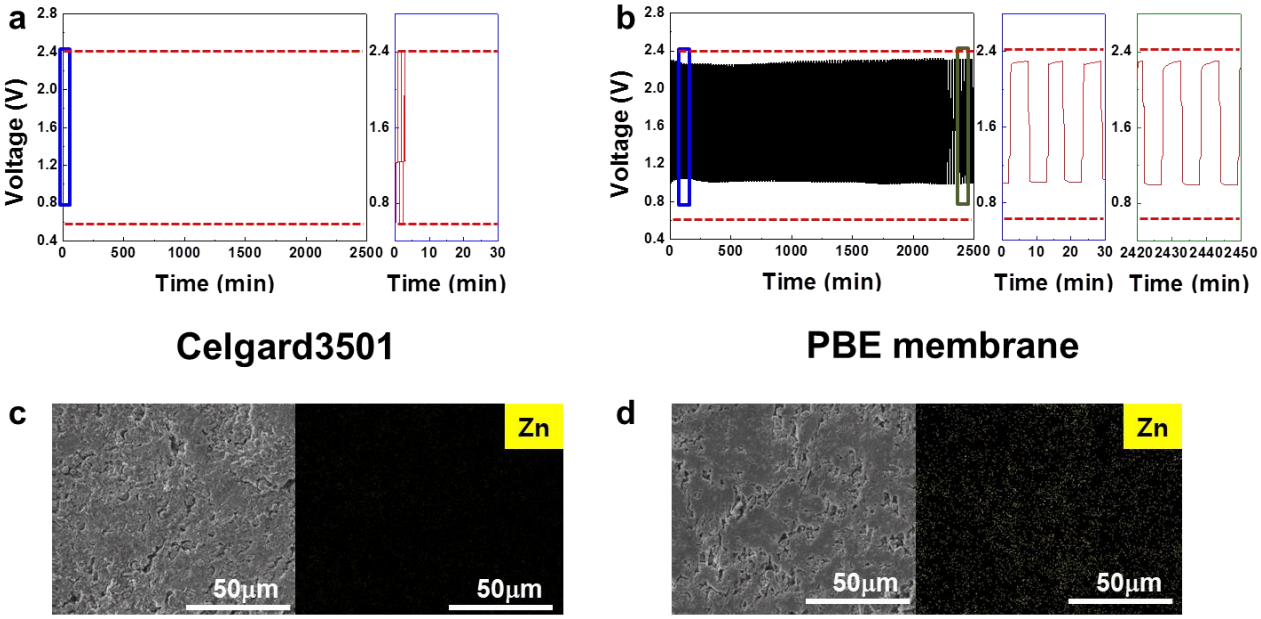

Figure S11. Electrochemical activity of Zn-air cells incorporating the reused separator membranes. (a),(b) For the reused Celgard3501 (obtained after the cycle time of 900 min in the 1st cell): (a) galvanostatic charge/discharge profiles of the 2nd cell; (b) SEM and EDS images of the air cathode surface after the 2nd cycling test. (c),(d) For the reused PBE membrane (obtained after the cycle time of 2500 min in the 1st cell): (c) galvanostatic charge/discharge profiles of the 2nd cell; (d) SEM and EDS images of the air cathode surface after the 2nd cycling test.